

Landslides
 DOI 10.1007/s10346-020-01609-x
 Received: 6 May 2020
 Accepted: 10 December 2020
 © The Author(s) 2021

Lene Kristensen · Justyna Czekirda · Ivanna Penna · Bernd Etzelmüller · Pierrick Nicolet · José Santiago Pullarello · Lars Harald Blikra · Ingrid Skrede · Simon Oldani · Antonio Abellan

Movements, failure and climatic control of the Veslemannen rockslide, Western Norway

Abstract On September 5, 2019, the Veslemannen unstable rock slope (54,000 m³) in Romsdalen, Western Norway, failed catastrophically after 5 years of continuous monitoring. During this period, the rock slope weakened while the precursor movements increased progressively, in particular from 2017. Measured displacement prior to the failure was around 19 m in the upper parts of the instability and 4–5 m in the toe area. The pre-failure movements were usually associated with precipitation events, where peak velocities occurred 2–12 h after maximum precipitation. This indicates that the pore-water pressure in the sliding zones had a large influence on the slope stability. The sensitivity to rainfall increased greatly from spring to autumn suggesting a thermal control on the pore-water pressure. Transient modelling of temperatures suggests near permafrost conditions, and deep seasonal frost was certainly present. We propose that a frozen surface layer prevented water percolation to the sliding zone during spring snowmelt and early summer rainfalls. A transition from possible permafrost to a seasonal frost setting of the landslide body after 2000 was modelled, which may have affected the slope stability. Repeated rapid accelerations during late summers and autumns caused a total of 16 events of the red (high) hazard level and evacuation of the hazard zone. Threshold values for velocity were used in the risk management when increasing or decreasing hazard levels. The inverse velocity method was initially of little value. However, in the final phase before the failure, the inverse velocity method was useful for forecasting the time of failure. Risk communication was important for maintaining public trust in early-warning systems, and especially critical is the communication of the difference between issuing the red hazard level and predicting a landslide.

Keywords Rockslide · Monitoring · Failure forecasting · Early warning · Temperature modelling · Risk management

Introduction

Unstable rock slopes pose a risk to communities and transportation networks because they may progressively develop into rock mass failures or rock avalanches. Monitoring slope deformation combined with early warning (EW) and evacuation is, in some cases, the only feasible method of risk mitigation. A relation between progressive slope acceleration and final failure may be used for setting alarm thresholds and forecasting purposes (Carlà et al. 2017), commonly based on the inverse velocity method for failure forecasting (Fukuzono 1985; Voight 1989; Crosta and Agliardi 2003). This method assumes that a linear, or close to linear, decrease of the inverse velocity over time can be found during acceleration, and the extrapolation of inverse velocity towards zero may predict the time of failure (Saito 1969). An assumption is that external forcing remains constant over time (Voight 1989). Changes in the slope geometry and periodically

changing factors such as precipitation or snowmelt that drives changing displacement rates may be a limitation on the use of inverse velocity methods for failure forecasting (Carlà et al. 2017).

Many studies on large and unstable rock slopes have shown seasonal fluctuations of the slope behaviour. For instance, La Saxe in Italy and Jettan in Northern Norway accelerate annually during snowmelt (Crosta et al. 2013; Blikra and Christiansen 2014). The landslide response to external forcing such as meteorological events and snow melting differs with the depth, volume, and type of material (effective permeability). While shallow landslides are commonly triggered by intense and short-term rainstorms, deep-seated landslides are normally affected by longer time scale seasonal fluctuations (Aleotti 2004).

Some studies suggest a link between permafrost thaw and slope instability, including large rock avalanches (Gruber and Haeblerli 2007). At the Piz Cengalo in Val Bondasca, Switzerland, blue ice was observed at the back scarp after the 1.5–2 million m³ failure in 2011 (Mergili et al. 2020) and small patches of ice in the back scarp were also observed after its 2017 3 million m³ failure (Walter et al. 2020). The possible processes causing destabilization when permafrost is thawing may be loss of bonding in fractures, ice segregation and volume expansion, and reduction of shear strength (Krautblatter et al. 2013). For Glacier Bay, SE Alaska, Coe et al. (2018) found a significant increase in rock avalanche frequency and size in recent times, where the increase appears to be correlated to rising air temperatures and permafrost degradation.

In Northern Norway, cosmogenic nuclide dating from the back scarp of the large unstable rock slope Gamanjunni 3 indicates initiation of the instability between 6.6 and 4.3 ka at c. 8 ka BP (Böhme et al. 2019). Slip rates decreased subsequently but are now significantly higher than the average since initiation, which is suggested to be an effect of recent warming. Hilger et al. (2021) discuss degrading permafrost as a driving mechanism for slope deformation for Gamanjunni, Mannen, and Revdalsfjellet in Norway, which are all situated at or above the lower limit of elevational permafrost. Their initial deformation coincides with the period of the Holocene thermal maximum (HTM), and their current displacement rates are higher than the reconstructed slip rates. Hilger et al. (2018) mapped and dated 6–9 rockslide deposits, in the Romsdalen valley below Mannen, and found a narrow cluster of events dating around 4.9 ka, also relating this to HTM.

Veslemannen was a small part of the larger Mannen unstable rock slope located in Romsdalen, Western Norway, at c. 1200 m a.s.l. and in a north-facing steep slope. On September 5, 2019, the most active part of the slope, with a volume of 54,000 m³ and 45–50° steep, failed catastrophically. Due to large precursor movements, *Veslemannen* was continuously monitored since October 2014. Displacements in *Veslemannen* were closely linked to rainfall events. The sensitivity to precipitation was time-varying with a lower sensitivity to rainfall in spring and an increased

sensitivity from summer to autumn (Abellan et al. 2017). This seasonal sensitivity pattern coincided with seasonal warming of the ground, implying that the thermal regime had an important influence on the slope dynamics. Indeed, *Veslemannen* was located in a zone of sporadic mountain permafrost (Magnin et al. 2019) and deep seasonal frost.

The Norwegian Water Resources and Energy Directorate (NVE) is responsible for the risk management of landslides in Norway and for the monitoring of unstable rock slopes classified with a high risk. Monitoring precursor movements is central for the EW system. NVE uses colour-coded hazard levels (green, yellow, orange, and red) and evacuations are undertaken at the red hazard level. During the 5 years of monitoring, *Veslemannen* evolved dramatically with increasing movements from year to year, in particular since 2017. Periodic accelerations of increasing frequency and magnitude caused a total of 16 warnings of the red hazard level, though only after the final one, the main parts of *Veslemannen* failed catastrophically. *Veslemannen* was the first forecasted rock mass fall in Norway.

The management was challenging from a geological point of view and burdensome for the affected community in the hazard zone. To set appropriate hazard levels and ultimately to predict a catastrophic failure required an understanding of the unstable slope, which was evolving along the way. We present here some lessons learned from this case, including the progressive development leading up to the failure, the relationship between the displacement, climate, and thermal control, and the risk management. The study aims to increase our knowledge on rockslide dynamics before failure and the thermal control in a setting of sporadic permafrost.

Setting

Geology and structure of the Mannen rockslide complex

The *Veslemannen* unstable rock slope was situated on a north-facing slope of Romsdalen, Rauma Municipality, Western Norway. Romsdalen is a 30-km-long over-deepened U-shaped glacial valley cut into the crystalline basement of the Western Gneiss Region, which was metamorphosed during the Caledonian orogeny (Fig. 1). Thinning of the ice sheet began around 15–13 ka, while a valley glacier extending to the fjord existed during the Younger Dryas (Hughes et al. 2016).

At Mannen, intensively folded high-grade metamorphic rocks are highly deformed and show clear evidence of gravitational fracture opening along the E-W subvertical foliation and nearly N-S fractures (Saintot et al. 2011, 2012; Dalsegg and Rønning 2012; Oppikofer et al. 2012). The Mannen unstable rock slope is a part of an even larger Mannen/Børa deep-seated gravitational slope deformation, which is currently inactive (Saintot et al. 2012). Henderson and Saintot (2007) deduced a translational sliding mechanism of deformation for Mannen, while Dahle et al. (2010) proposed that the deformation might be a wedge failure with steps along the sliding surface. The structural and topographic conditions are promoting slope collapses, and the Romsdalen valley has the highest spatial density of post-glacial rock slope failures in Norway (Saintot et al. 2012).

Mannen is one of the seven continuously monitored high-risk sites in Norway, as both the probability and the consequences of a failure are large. The uppermost part (scenario C—3 mill m³)

moves about 2.5 cm/year NE with a dip of 60°, while scenario B (12 million m³) moves about 0.5 cm/year N with a dip of 20° (scenarios in Fig. 2). Real-time instrumentation and monitoring of Mannen were initiated in 2009 and include a network of eight GNSS antennas, two lasers, seven extensometers, four tiltmeters, two 120-m-deep DMS borehole instrumentations, a web camera, a meteorological station, and a ground-based interferometric radar system (GB InSAR). No in situ instruments were initially placed on *Veslemannen*, and the area was not in view from the original GB InSAR system. The high velocities in *Veslemannen* were therefore not discovered until 2014 when a new GB InSAR system was put in place.

Veslemannen was outlined from measured displacement rather than geological structures. The upper boundary of *Veslemannen* is located at 1220 m a.s.l., 60 m below a plateau, and was marked as a snow-filled open fracture (Fig. 3). Below the back fracture, some parallel transverse fractures were found and most of the movement and the final failure of *Veslemannen* occurred along one of these fractures, leaving the uppermost part behind. Its western limit extended along a narrow gully carved along a regional tectonic fault, while the eastern one was more diffuse eastern and followed a longitudinal ridge in the slope. *Veslemannen* had a general slope angle of 45–50° and a steep frontal part of 70°. The upper part was highly fractured with loose blocks up to several meters. The middle part contained crushed rock, but the original E-W vertical to subvertical foliation could still be seen before the failure. The steep lower part or toe area consisted of more intact rock and included a 15–35-m-high pinnacle, *Spiret*, or the Tower that was interpreted to be a key block stabilizing the upper part of the slope. The volume of *Veslemannen* was estimated to be around 120,000–180,000 m³ (Skrede et al. 2015), though the failure in September 2019 involved only 54,000 m³.

Climatic settings and ground temperatures

From 2010, a meteorological station was operated at the upper plateau. The average air temperature for Mannen (1280 m a.s.l.) is –0.2 °C (8 years of data), and an annual precipitation around 2000 mm (www.Senorge.no). In relation to the normal period 1961–1990, average air temperatures are 1–2 °C warmer today, based on nearby climate stations. At the plateau, the ground is usually snow-covered from November to late June, with snow thickness typically reaching 3–4 m in late winter.

Near the climate station, shallow borehole thermistors down to 3 m depth all recorded average temperatures of > +2 °C. In *Veslemannen* itself, ground temperatures were recorded in 2015 in fractures in the uppermost part. Temperatures below the snow were stable between mid-March to early May, recording temperatures between –1.3 and –2.3 °C, indicating the possibility of permafrost pockets (Haeberli 1973). *Veslemannen* with its steep north-facing slope received almost no direct sunlight. Snow cover at most of *Veslemannen* was thinner than at the plateau, and ground surface temperatures were most likely colder than on the plateau. In 2016, two rock-wall temperature loggers were installed in the back scarp of Mannen in a northerly and easterly direction. Mean annual rock-wall temperatures are +1.2 °C in the northern slope and +2.5 °C in the easterly directed part of the scarp (Magnin et al. 2019). In view of the recent warming since 2000, rock-wall temperatures close or below the freezing point in recent past are probable. A statistical model for rock-wall temperatures



Fig. 1 The location of the Mannen rockslide in Western Norway. Inset: A photo of Romsdalen with the location of Mannen

indicates discontinuous to sporadic permafrost in the rockslide area (Fig. 2). Electrical resistivity soundings combined with lab testing of electrical resistivity of rock samples from Mannen (Dalsegg and Rønning 2012; Etzelmüller (unpublished data)) indicate high-resistivity areas in and below the Mannen scarp, and permafrost in deeper parts of the mountain.

Methods

Displacements and kinematics

Ground-based InSAR system

The main method for monitoring surface deformation at Veslemannen was a ground-based (GB) InSAR system from LiSALab Ellegi. GB InSAR has been widely used to characterize and monitor landslides (Bertolo 2017). The radar uses the k_u band and the parameters used at Veslemannen are listed in Table 1.

With this frequency, phase wrapping occurs if movement exceeds 4.4 mm from image to image. Therefore, the image processing average interval was changed on the system according to the measured displacement rates and was typically from 4 h to a few minutes. When velocities were high, the running speed of the radar was also increased to avoid phase wrapping. The uncertainty of the measurements using a normal workflow is about ± 0.5 mm, but this value increases when only a few images can be included in the temporal averaging (e.g. during crisis situations) and when snow accumulated in the slope, or occasionally when the software was unable to properly correct for atmospheric effects. The LiSALab Main Lisa Mobile software was used to process the data and display the results. Interferograms and cumulated interferograms were georeferenced and transformed into raster files to be displayed in a geographical information system (GIS) using the position and view direction of the radar in combination with a 1×1 -m digital elevation

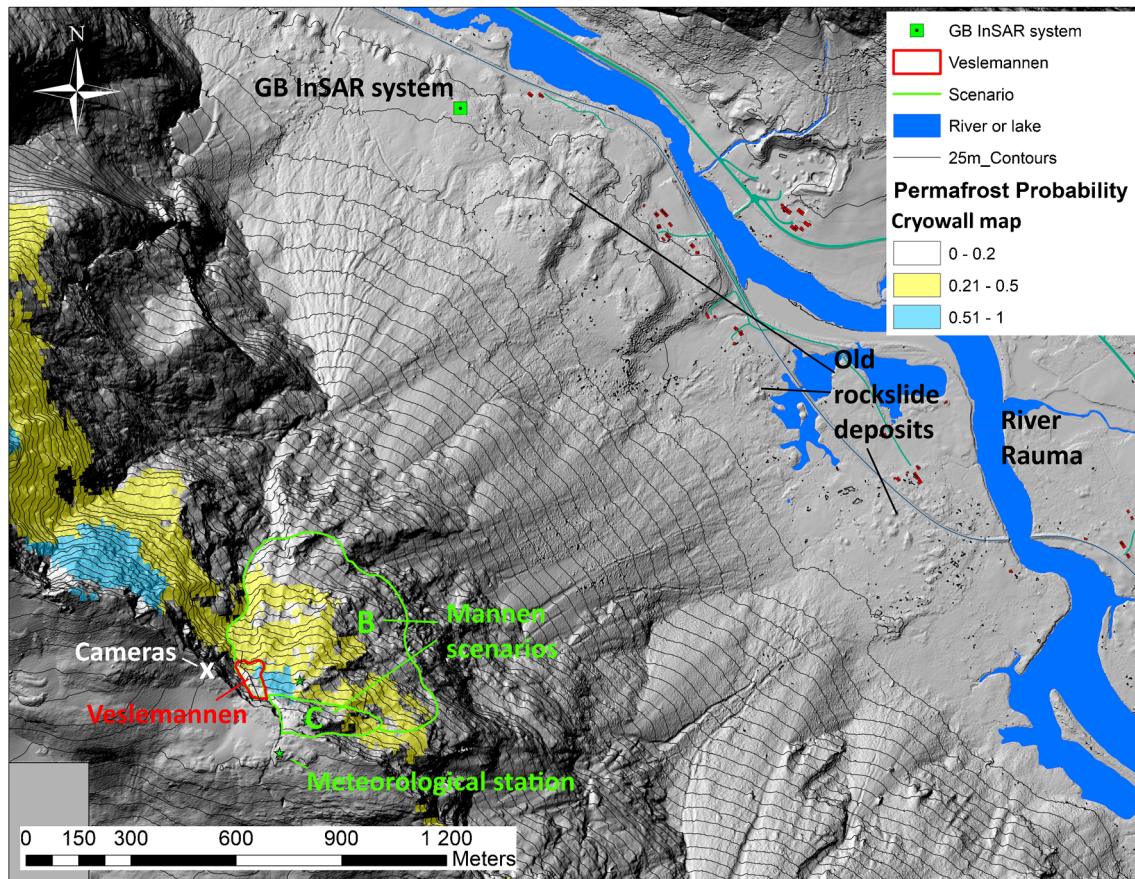


Fig. 2 A hillshade map showing Veslemannen and the Mannen scenarios. The positions of the radar system and the meteorological station are indicated. The blue and yellow colours in the slope show modelled probability for permafrost from Magnin et al. (2019)

model (DEM). Time series of displacement or speed for selected pixels were analyzed. The movement is measured in the line of sight (LOS), which is assumed close to the direction of movement in the case of Veslemannen. The radar was continuously operated from October 6, 2014, from the valley floor at Lyngheim (Fig. 4, location Fig. 2).

Extensometers

Extensometers measured movements in the upper part of Veslemannen from late 2014 to 2017. The instruments were from Temposonics, R-series analogue (RH-M-1000M-D60-1-A01), with a sensor length of 1 m. They were built into a solid steel pipe and bolted across fractures, recording the movement in 1D. Their noise level was less than the GB InSAR measurements but showed similar trends in movement. The extensometers were repeatedly expanded beyond their range due to a large movement and had to be replaced or repositioned. As the terrain got increasingly dangerous, NVE stopped maintaining them in late 2017. In 2018, the block where the extensometers were mounted on failed.

Time-lapse cameras

From June 2016, an AXIS Q6115-E Network Camera was operated from the plateau, looking down to the moving area (Fig. 4, location Fig. 2). It could be controlled (turned and zoomed) remotely and

took a photo (1920 × 1080 DPI) every 2 h with a set view to Veslemannen. The images were stored when day light and continuous recording was enabled, allowing for obtaining movies for instance during rock fall events.

In 2018, a 42-MP deformation camera from Geopraevent was installed at a position close to the AXIS camera. It took photos every 2 h. Selected images were processed, and the system performed a daily deformation analysis by pixel recognition (Fig. 3).

3D models and volume calculations

A series of 3D models from four different data sources were used:

- 1) 2009 (unknown date): An airborne LIDAR scan, covering the entire area of Mannen
- 2) October 19, 2015: Photogrammetric point cloud and DEM made from images taken from a helicopter
- 3) August 15, 2019: Photogrammetric point cloud and DEM made from drone images
- 4) September 6, 2019 (after the September 5 failure): Photogrammetric point cloud and DEM made from drone images>

The three photogrammetric point clouds have been manually cleaned to remove errors and artefacts, and aligned to the LiDAR

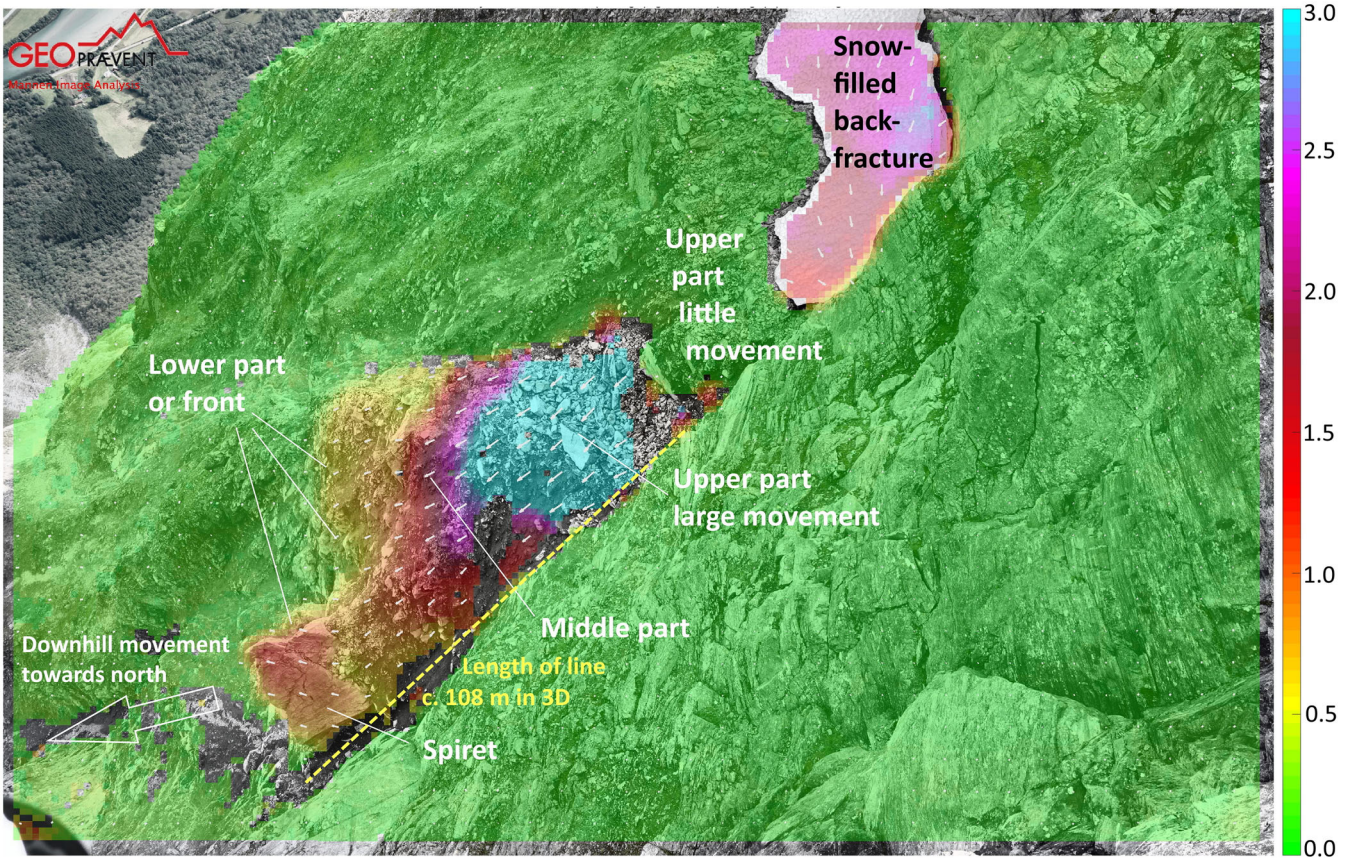


Fig. 3 A photo of Veslemannen looking down from the plateau above. The colours indicate displacement in a pixel scale where blue and purple are the largest movements while green is stable ground. The arrows indicate the direction of movement, calculated by Geopraevent. The position of the camera is marked on Fig. 2

DEM in CloudCompare (CloudCompare 2020), first by picking equivalent point pairs and then using an iterative closest point (ICP) algorithm, allowing a change in scale. When necessary, a mesh has been built from the point clouds. DEMs from the point clouds have been interpolated subsequently in CloudCompare.

Table 1 Parameters used at the LiSALab radar

Rail length	3 m	
Central frequency	17.2 GHz	
Bandwidth	80 MHz	
Nr. of frequencies	2501	
Steps along the rail	601	
Image acquisition time	1.5–8 min	
Processed image range	600–2300 m	Range resolution 1.9 m
Processed image azimuth	± 850 m	Azimuth resolution in 2 km: 6 m
Image resolution	1000 × 1000 pixels	

Ground temperature modelling with CryoGrid 2D

A transient 2D heat flow model, CryoGrid 2D (Myhra et al. 2017), was used to model evolution of the subsurface temperatures in Veslemannen. Ground temperatures are obtained by solving a 2D heat diffusion equation with the material- and temperature-dependent thermal parameters, such as the effective volumetric heat capacity and the thermal conductivity. The thermal parameters are functions of volumetric contents of ground constituents (water, ice, mineral, organic, air) and their individual thermal properties (Westermann 2013). The latent heat effects due to water/ice phase transitions are included in the effective volumetric heat capacity term.

In CryoGrid 2D, the MATLAB-based finite element solver MILAMIN package (Dabrowski et al. 2008) generates an unstructured triangular mesh with a defined maximum triangle area for a given slope geometry and is used for space discretization, whereas time discretization is based on a finite-difference backward Euler scheme. A detailed description of the equations used in CryoGrid 2D is given in Myhra et al. (2017). CryoGrid 2D is entirely a conductive model, so convective water- or airflow is unaccounted for. Both are likely to modify the thermal regime in the fractured subsurface of Veslemannen. The model is constructed as a 2D slice through a slope and assumes a translational symmetry along the third dimension.



Fig. 4 The GB InSAR system before a permanent hut was built, and a time-lapse camera at the edge of Romsdalen, looking down at Veslemannen

Slope geometry, stratigraphy, and boundary conditions

The surface elevation was extracted from the 2009 DEM along an approximately north-south transect. The subsurface is divided into six distinct classes based on the geological profile with estimated mineral/air/water content (Fig. 5). No organic matter and a freeze curve for sand are assumed for all the subsurface regions. To account for the larger temperature gradient close to the surface, nodes are constructed at the upper boundary with a distance of 0.05 m, while the maximum triangle area for the part with Veslemannen is 0.05 m² and the bedrock layer has depth-dependent spacing (0–2 m depth: 0.1 m²; 2–50 m depth: 1 m²; > 50 m depth: 50 m²).

A bedrock thermal conductivity of 2.5 W m⁻¹ K⁻¹ is used, which is a common value for quartz-rich bedrock (e.g. Robertson 1988). The model is constructed with zero flux boundary conditions along the right and left boundaries, while a geothermal heat flux of 50 mW m⁻² (Slagstad et al. 2009) is used at the lower boundary at 6000 m depth.

Model forcing

CryoGrid 2D requires ground surface temperature (GST), i.e. temperature below snow cover, as model forcing since the model includes only the ground domain. The model was run weekly from September 1, 1864, until December 31, 1956, using GST obtained from surface air temperatures (SAT), found by correlating air temperatures from <http://www.senorge.no> to nearby meteorological stations and accounting for the insulating effect of snow by using Nf-factors (forcing zones in Fig. 5). The snow thickness was estimated for selected forcing zones by studying weekly images from the Axis camera and by correlating with the snow depth data from the mountain top in the period 1957–2018. The 1957–2018 SAT and snow data were used to force a 1D CryoGrid 2 model (Westermann et al. 2013), and the output from the uppermost cell in the ground domain was subsequently employed as forcing in CryoGrid 2D.

The supplementary material includes a description of the model initiation, model runs, and sensitivity testing with varying water content. The modelling results and sensitivity tests are shown as movies of different time steps.

Results

Veslemannen evolution and failure

Displacement in Veslemannen prior to failure

The displacements in Veslemannen prior to 2014 are unknown, but the deformation probably started much earlier. From October 2014 to the failure in 2019, the total displacement in Veslemannen was up to 19 m in the upper parts and 4–5 m in the toe area (time series in Fig. 6a and location of the points in Fig. 7). Typically, movements started slowly in June and increased until around October when freezing conditions set in, and very little displacement was measured during winter seasons. The cumulated displacement on an annual basis was approximately similar during 2014, 2015, and 2016, with about 0.8 m in the upper part and 0.1 m in the toe area. The movement tripled in 2017 (1.9 m in the upper part and 0.26 m in the toe area) and more than quadrupled in 2018 (9 m in the upper part and 1.2 m in the toe area). At the date of failure, displacement in 2019 was 5 to 12 times higher than at the same date in 2018 (Fig. 6b).

The measured displacement was typically six to eight times higher in the upper than in the lower part. This relation changed as the difference was reduced in the final phase towards the final failure (Fig. 8). The last day before the failure the movement was almost uniform in the upper and lower parts of the instability.

Figures 3 and 7 clearly show that the area of large displacements does not extend to the snow-filled back fracture, as originally assumed. During the first years of monitoring, the radar data had little view to this uppermost area, but as the topography changed, it was clear that the movement mainly occurred along a transverse fracture lower in the slope. This was confirmed from time-lapse images, which were not available when the original scenario was estimated. The failure took place along this fracture, and the uppermost part towards the snow-filled back fracture remained in place. Some movement was still recorded above the failed part until freezing stabilized the area in late 2019. In the summer and autumn 2020, a series of minor failure has occurred towards the snow-filled back fracture.

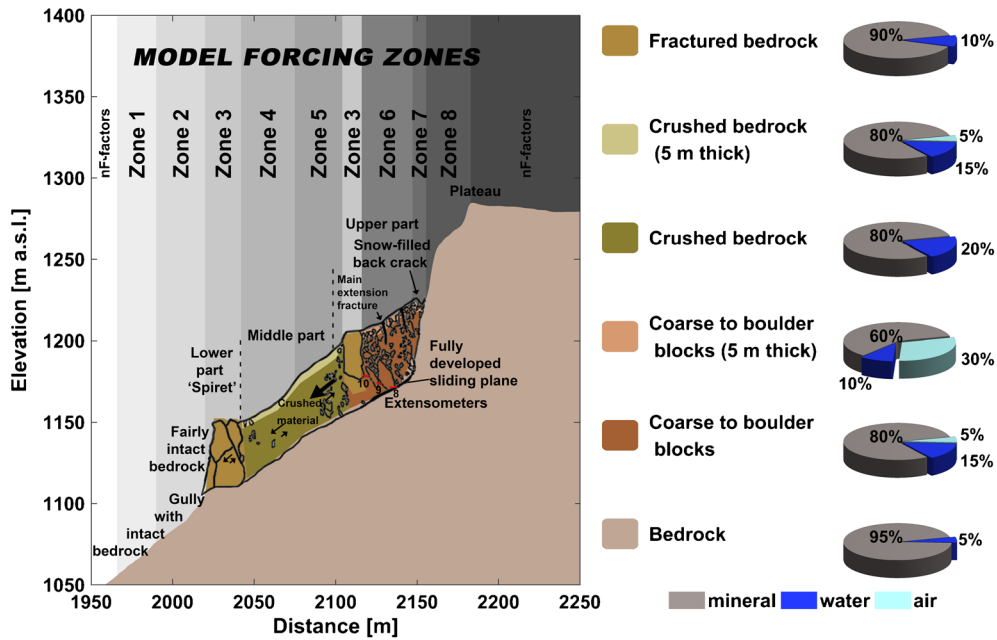


Fig. 5 Geometry and stratigraphy used in the CryoGrid 2D model: Six subsurface classes are drawn on a geological profile, and the compositions of each class are shown on the adjoining pie charts. Rock wall above the instability (zone 8) is usually snow-free. Zone 7 represents a snow patch, with an assumed constant GST of 0 °C throughout the modelling period. Snow cover in zone 6 is thick and melts late in the season. Zones 3 (note there are two of these) are wind-exposed and have limited snow cover during winters. Zones 4 and 5 are snow-covered during winter seasons

Rock falls and change in topography prior to the failure
 Rock falls were frequent from Veslemannen and were often associated with acceleration phases. In 2018 and 2019, substantial parts of the instability failed as rock falls or rockslides, and movie examples documenting a few of these events are included in the

supplementary material. Over time, the changes due to large movement and rock falls were so significant that the existing topographic map was not accurate. In August 2019, a new terrain model was created from drone images and compared with a point cloud from October 2015 (Fig. 9). The surface is lower in the upper

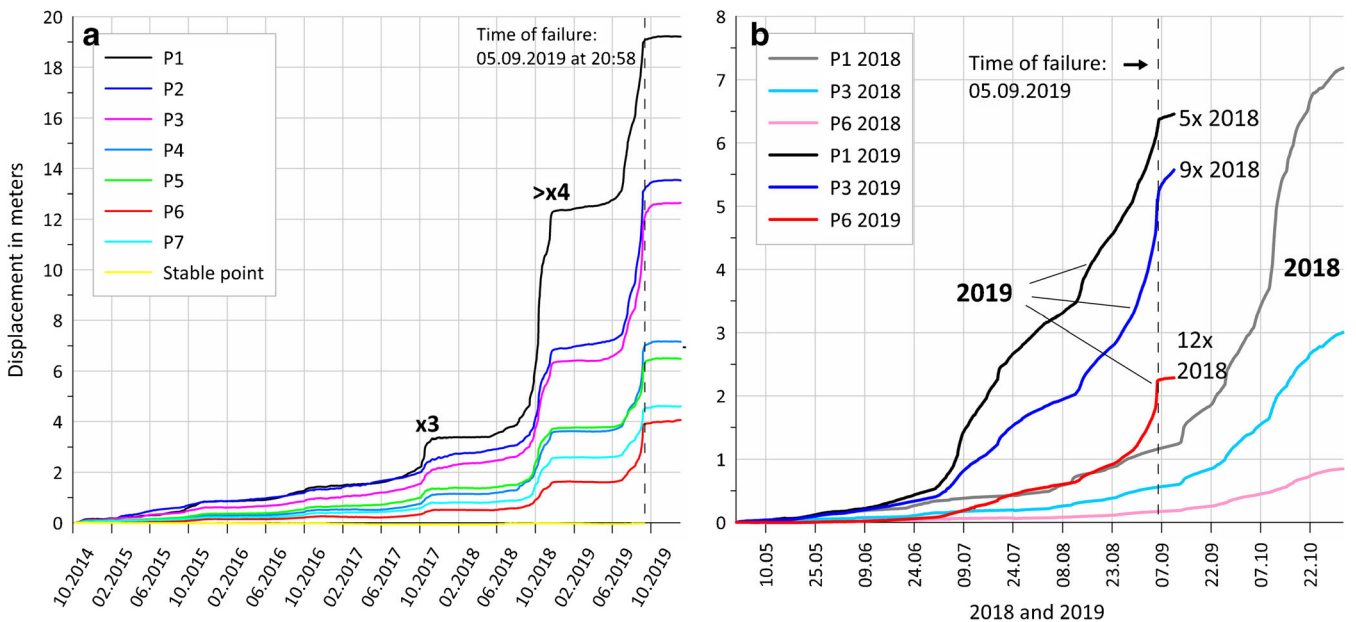


Fig. 6 a Cumulated movement in radar points from 2014 to the failure. b Comparison of the movement in selected radar points in 2018 and 2019

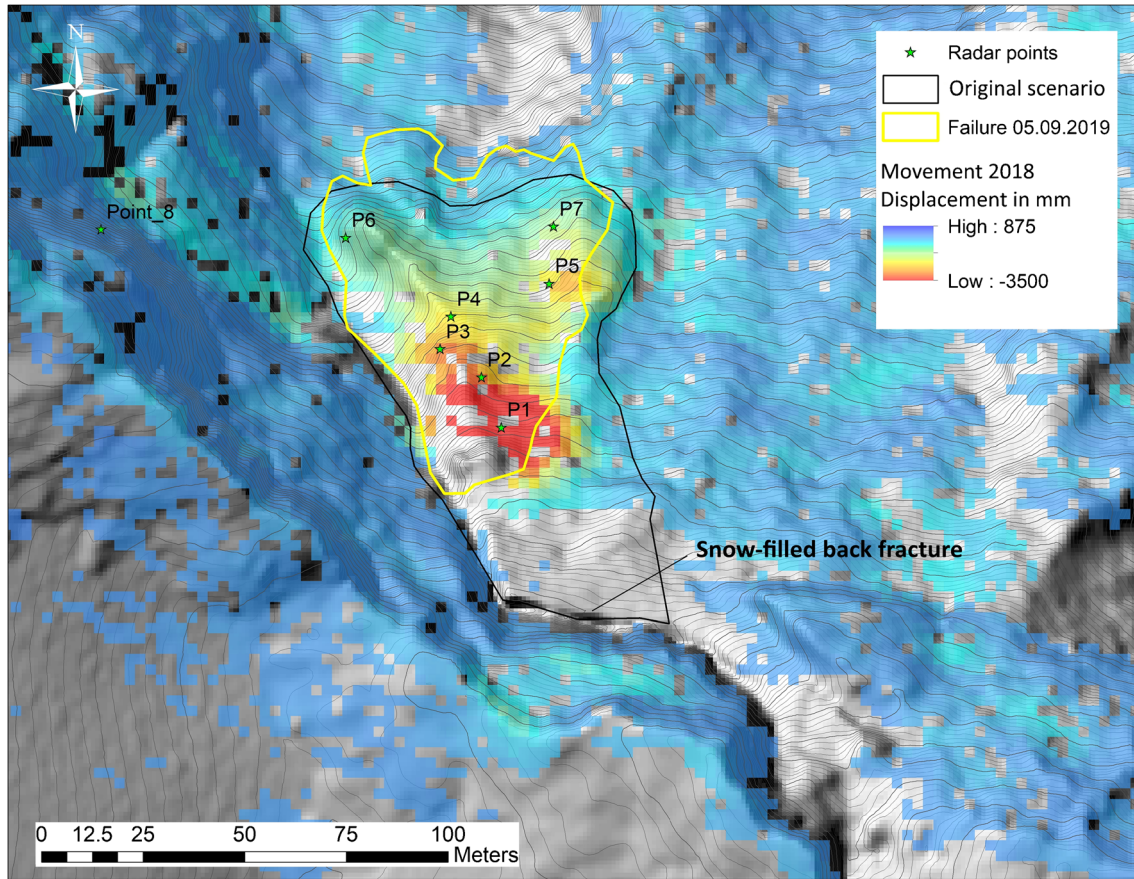


Fig. 7 Cumulated displacement map, showing the points where time series were exported. The original scenario and the area that failed are drawn

part of the slope while some elevation gain is seen in the lower parts. About 15,000 m³ were removed by rock falls in this period.

The rock mass fall on September 5, 2019

A slow acceleration of the rock slope was observed from around August 23, 2019, which was not related to rain or snowmelt (Fig. 10). At midnight on September 5, 2019 (the night before the failure), a rainfall set in, and about 19 mm of rain was measured from midnight to around 15:00. This caused a sharp acceleration, overprinting the ongoing acceleration. Figure 11 shows that the acceleration took place in three distinct steps, at 06:00, 10:30, and

14:30. At about 15:00, the velocities were 1.5 to 1.8 m/day and after that phase, wrapping started consistently to affect the radar images, and the velocities on the figure are no more reliable. However, we interpreted the interferograms as continued acceleration, as it was possible to estimate the increasing velocities by counting the fringes (indicating phase wrapping) on the interferograms. From 20:00, i.e. an hour before the failure, the plot shows no velocity, indicating a complete loss of coherence in the radar images and random positive or negative values for the points.

At 20:58, the toe area (*Spiret*) failed catastrophically, and the most active area followed within some minutes. Unfortunately, the

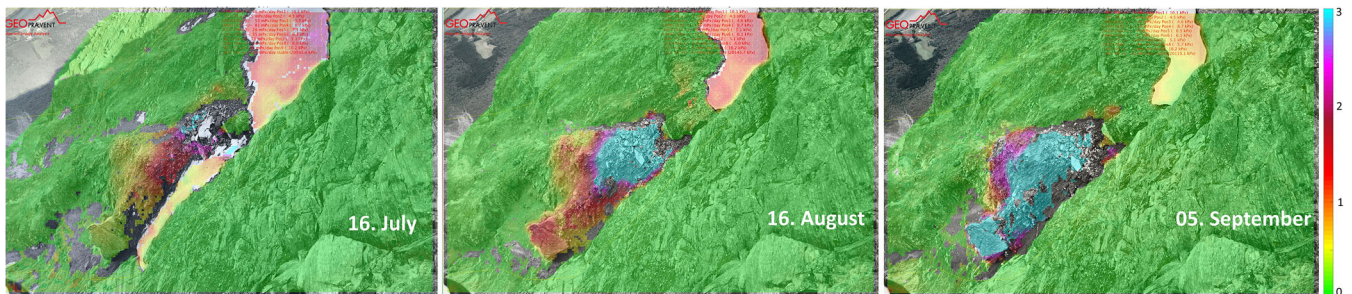


Fig. 8 Displacement recorded from the Geopraevent camera on Veslemannen in the months before the failure. Velocities increased and the movement became increasingly uniform in Veslemannen towards the failure

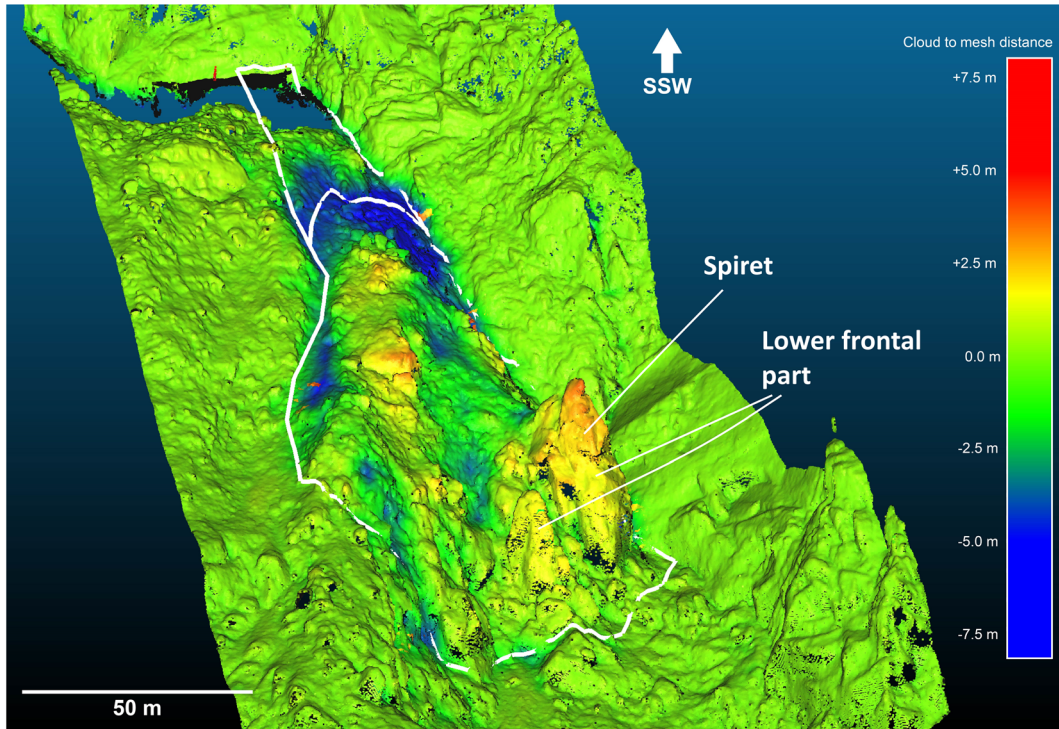


Fig. 9 Surface change from 2015 to August 2019. The surface lowering is blue while the elevation gain is yellow to red. The white lines show the failure area and the original scenario of Veslemannen

NVE cameras did not record the event, as fog and darkness remained on the slope, which is why there was movement in some obscured the view. Some rock fragments and loose material of the radar points after the failure. The following days, rock falls

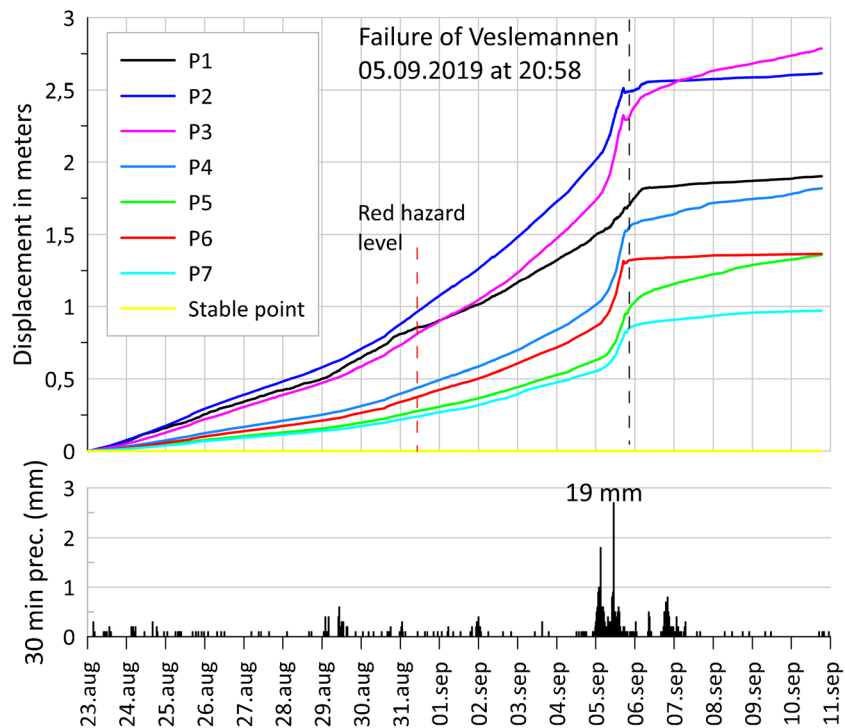


Fig. 10 Cumulated movement and precipitation from August 23 to September 11

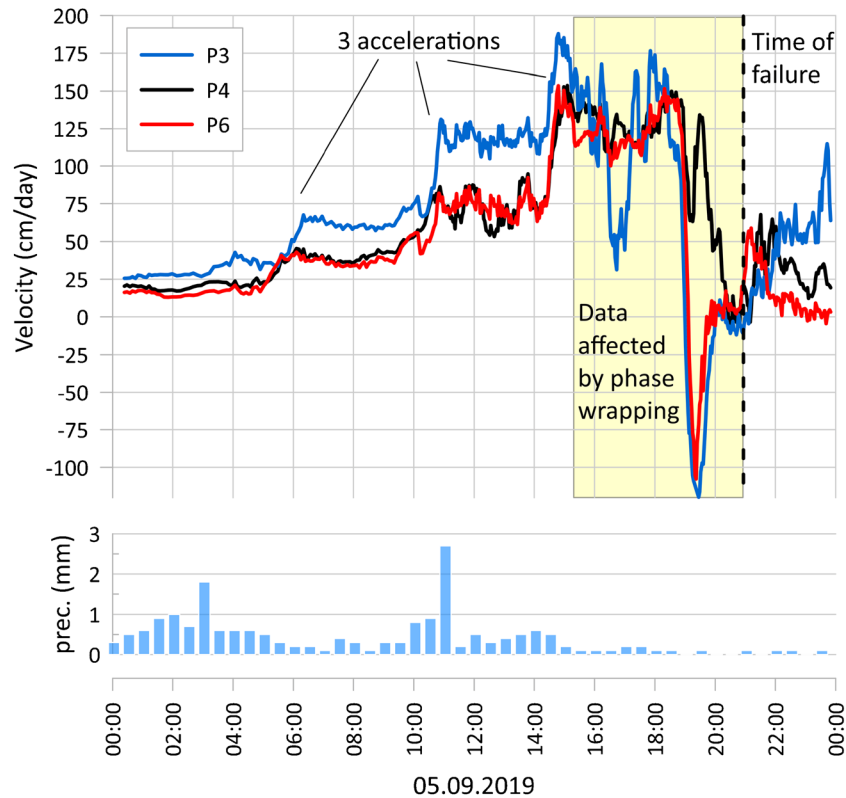


Fig. 11 Velocities and precipitation from three selected radar points at the day of the failure

occurred almost continuously, but the activity slowed down as it became colder. Figure 12 shows the Veslemannen area before and after the failure.

By comparing the DEMs just before (August 15, 2019) and after (September 6, 2019) the rockslide, a failure volume of 54,000 m³ was detected. This was less than the original estimate of 120–180,000 m³, mainly because the affected area was smaller than the original scenario (Fig. 7) and partly due to mass loss from rock falls before the final failure. The depth to the sliding plane was also less than anticipated. Figure 13a shows the movement on the last 2 days before the failure, and Fig. 13b shows the change in surface elevation after the failure. The maximum surface lowering from the failure at 45 m was observed at *Spiret*. Typically, the depth of failure was 14–20 m.

The basal plane of failure appears to form an extension of the gully below. The exposed sliding plane is rugged. In the middle part, the exposed bedrock appears irregular with stepwise breaking, and with the steeply dipping anti-slope foliation still visible. On average, the exposed failure surface is dipping 50° NNV (342°).

The runout was shorter than expected, and fortunately, no buildings were impacted by the rock mass fall. Some boulders and blocks, mainly from *Spiret*, reached the large fan below as shown by the Norwegian TV-channel TV2 (<https://www.tv2.no/v/1492014/>), which had a camera in the valley, but the main part of the mass was deposited in the steep gully. The rockslide deposited coarse material on the gully sides leaving a very coarse frontal deposit at the end of the gully just over a large fan. Here the deposit reached 16 m in thickness. Figure 14 shows the elevation

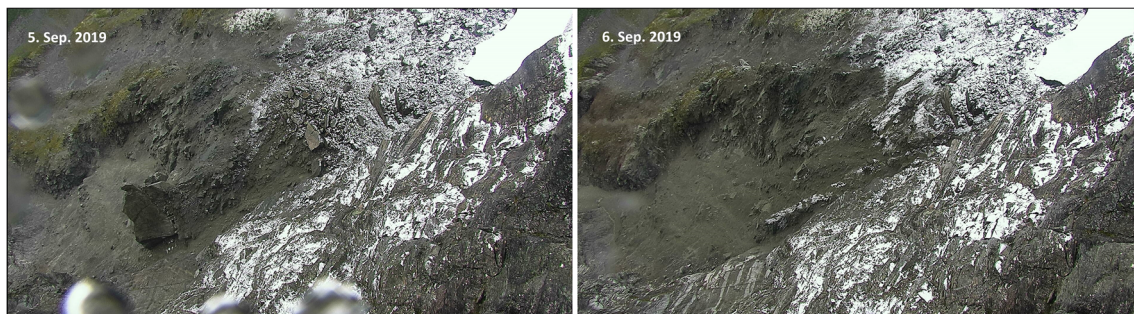


Fig. 12 Photos from the Axis camera looking down at Veslemannen from before and after the failure

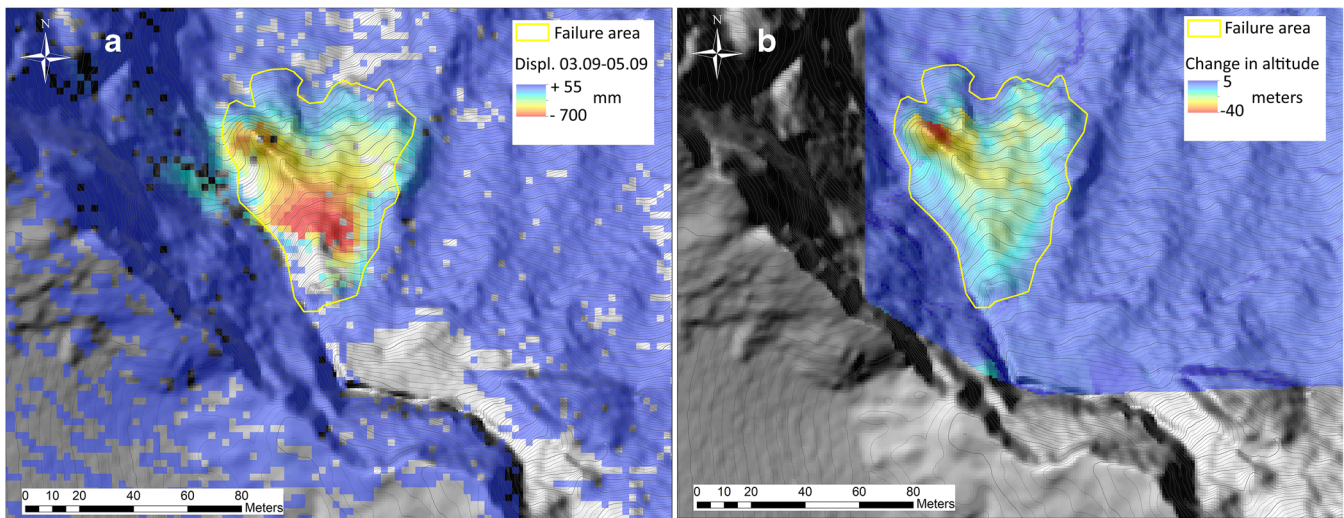


Fig. 13 a Displacements the last 2 days before the failure. b Elevation changes before and after the failure

changes and a photo of the deposit. The sediment deposited in the gully was around 66,000 m³, which is larger than the failed volume (54,000 m³). This is caused by volume increase due to rock fragmentation.

Veslemannen thermal regime

The temperature modelling indicates significant warming in the subsurface of Veslemannen from 1970 to today (Fig. 15 and supplementary material). The model was run on the topography from the 2009 terrain model. As the terrain changed significantly from displacement and rock falls from 2017, we show the modelling results from 2016 as the most recent. Ground temperature warming is especially evident since 2000. In 1970, permafrost was probably present in Veslemannen, while only pockets very close to 0 °C remained in 2016. In 1990, a talik or unfrozen area in the ground is modelled in the middle part at approximately 1210 m a.s.l., where the permafrost body has become decoupled into an upper and a lower colder zone. The colder zones are associated with areas with low snow cover, such as around the lower *Spiret* and the upper steep rock wall, which acted as a “refrigerator” to the ground (Myhra et al. 2017). The instability was subject to deep seasonal frost. Figure 15c shows the temperatures in the coldest period (April), with a thick frozen surface layer, and Fig. 15d shows that even in August, a frozen layer was probably found near the surface of Veslemannen. The warmest subsurface temperatures were modelled to occur around November.

Discussion

From progressive deformation to failure

The failure of Veslemannen is the result of a long history of slope deformation. An offset of 60 m between the top of the plateau and the upper part of the instability already before the monitoring started in 2014, may partly be caused by an earlier slope deformation. From 2017 and up to the rock mass fall on September 5, 2019,

displacement increased drastically from year to year (Fig. 6), clearly indicating a progressive damage and weakening.

The significant differences in the measured displacements rates and observed rock damage give a hint about the controlling processes. Larger displacements caused an almost complete disintegration of the bedrock in the upper and middle parts of the instability. In contrast, 6–8 times slower displacement rate in the toe area, including *Spiret* (Fig. 9), resulted in (or was caused by) more intact rocks. This indicates an accumulation of stress at the toe of the unstable rock mass, also proposed by Saintot et al. (2011) and Skrede et al. (2015).

Unfavourable pre-existing geological structures were probably the main reason why the failure did not occur earlier, despite the large displacement rates. At Veslemannen, the foliation dips steeply into the slope and no favourable outgoing sliding planes were observed. In the detailed structural analysis of Mannen, Saintot et al. (2011) did not observe a clear sliding surface and proposed that several moderate to shallow dipping joint sets guided its development. Our study shows that the final failure was achieved by a progressive weakening of the foot of the rock mass. We observed a rugged exposed sliding surface that does not appear to follow any common structures (Fig. 12).

Between 2018 and 2019, several episodes of significant accelerations of the entire mass were initiated by rock falls occurring at the foot of the instability, without being triggered by precipitation. This includes an event where a large block was observed to “shoot out” from the front. The stress release caused the entire rock mass to almost immediately advance forward and later gradually to slow down. These episodes as well as the stress transfer from the upper part gradually weakened the lower toe zone. The failure of existing rock bridges in the toe zone is highlighted by the development of more uniform displacements throughout the rockslide during the last phase (Figs. 7 and 10). As the lower part of the instability (*Spiret*) failed, most of the remaining fractured rock mass lost its basal support and progressively collapsed.

This case demonstrates that under complex structural conditions, hazard management can be challenging. Numerous episodes

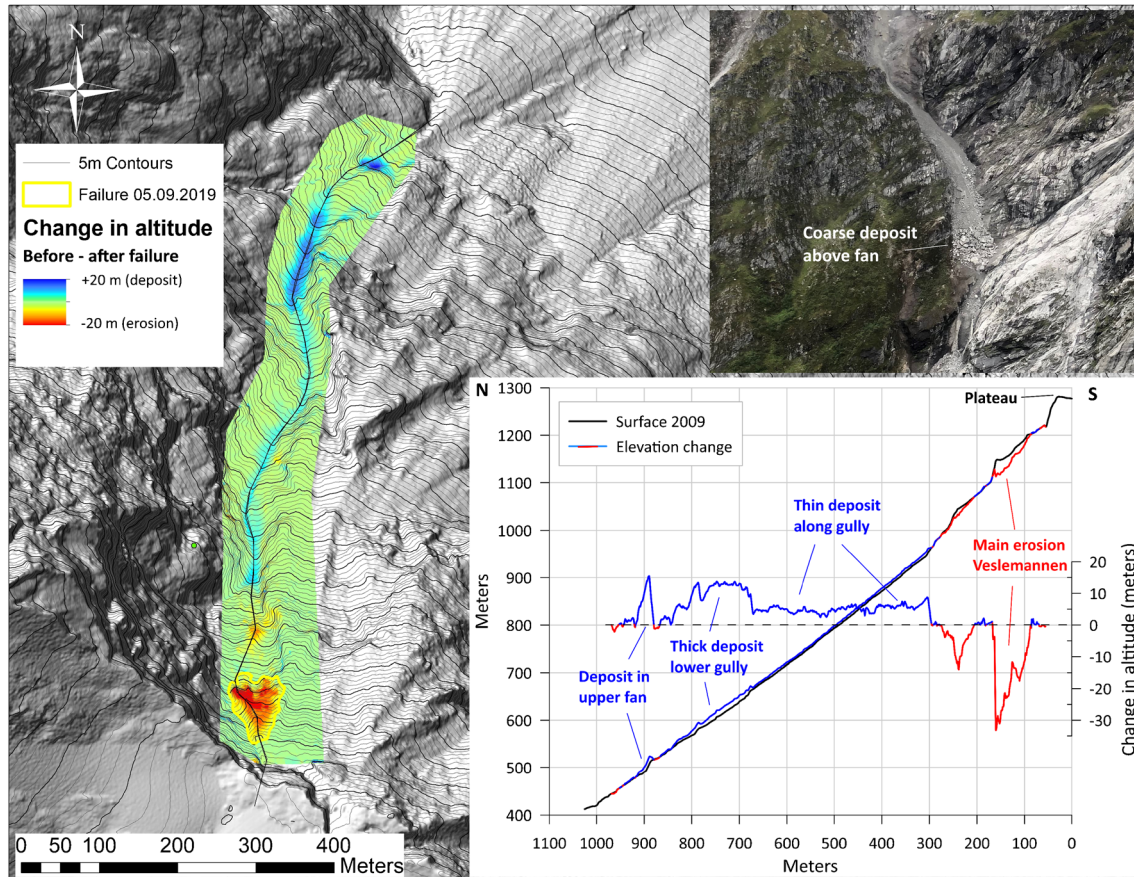


Fig. 14 Surface changes due to the failure. Most sediments were deposited in the gully above the fan. The profile shows erosion and deposition from the plateau to the upper fan and the inset photo shows a coarse deposit forming a “plug” above the fan

of acceleration on the rock mass may be required before sufficient structural damage at the front allows for a failure to occur.

Precursor movement controlled by cyclic loading: water supply and thermal conditions

Displacements prior to the failure of Veslemannen were highly influenced by water supply from rainfall or snowmelt. Peak velocities in the upper part of Veslemannen were typically measured 2–12 h after a peak in precipitation, while the response in the toe area was usually delayed more than 24 h. Accelerations were caused by temporary changes of properties in the sliding zone, and with the highly fractured bedrock and shallow depth at Veslemannen, we assume that no significant water table could build up in the instability. The clear correlation between the water influx and movements is interpreted to be caused by saturation or transient increased pore pressure in the sliding zone at the transition to the more intact rock below.

A clear trend of increased sensitivity and reaction to precipitation was observed every year from summer to autumn. Even at days of rapid snowmelt, movements in Veslemannen only increased a little during the spring season (Fig. 16). From late summer to autumn, rainfall or melting from an early snowfall would cause a steep acceleration, and the sensitivity to water supply increased each year until around October. This is a type

of time-varying effect, where the response to the driver varies with the season (Abellan et al. 2017). The sensitivity is related to ground temperatures as indicated in Fig. 17, and we hypothesise a thermal mechanism for the observed time-dependent slope sensitivity to rainfall.

The temperature modelling of Veslemannen was an attempt to approach this issue. Figure 2 and Fig. 15 indicate that Veslemannen was located at a particularly cold section of the slope. From 1970 to 2016, the area warmed considerably, and a layer of year-round unfrozen ground lying in permafrost (*talik*) formed at the upper part of the slope where the failure occurred. The modelled temperatures in 2016 were close to zero ($-0.5\text{ }^{\circ}\text{C}$), so the existence of permafrost at the time of failure was uncertain. No ice was observed at the failure plane at the drone images taken the day after the failure. We propose that recent warming and permafrost degradation could have played a role in the destabilization of Veslemannen, though we are not able to demonstrate a recent increased failure frequency. A feedback mechanism, where increased fracturing allowing more water to percolate and thus heat transfer by advection (not included in the model) and further warming and destabilization, is likely.

What is clear from the model is the deep seasonal frost, as exemplified with temperatures from April and August 2016. Even during August, a frozen zone remains. The bedrock was highly

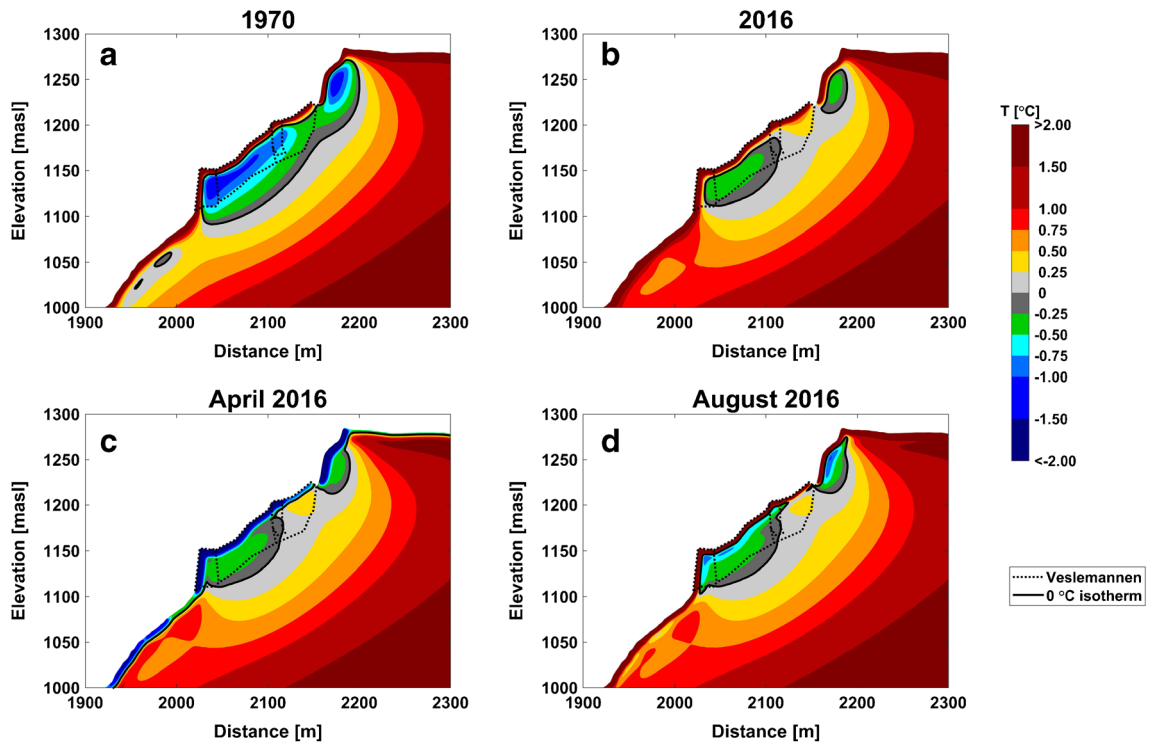


Fig. 15 Ground temperatures modelled for Veslemannen. a maximum temperature in 1970, b maximum temperature in 2016 (around November), c mean temperature in April 2016, and d mean temperature in August 2016

fractured, but we assume that the upper layer became saturated with ice during autumns and was impermeable for water infiltration during winters. For this reason, most of the water released during snowmelt in early summer was unable to reach the

sliding plane and influence the movement significantly. During the late summer, the pore-ice gradually melted, and rain was able to freely reach the sliding plane, causing Veslemannen to be increasingly sensitive to precipitation. The warmest conditions

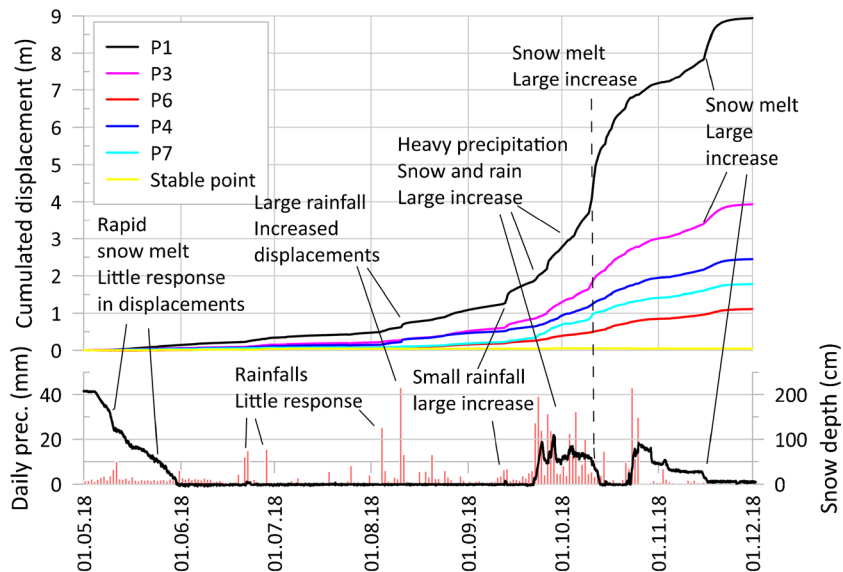


Fig. 16 Cumulated displacement, precipitation, and snow depth from May to December 2018. In 2018, early snowfalls and subsequent melt from September and onwards highly influenced the water supply and displacement rates. The spring snowmelt hardly affected the displacements, while rainfalls or snowmelt late in the season caused large increases in the displacements

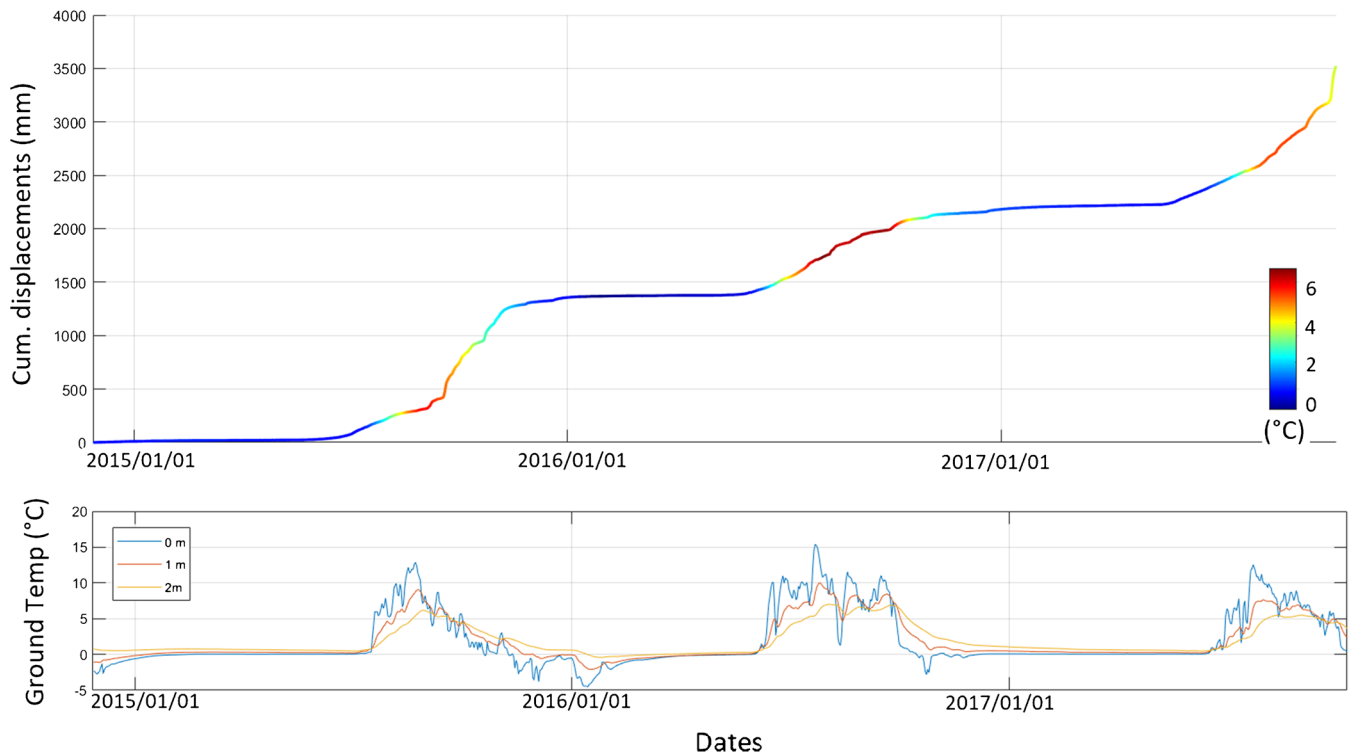


Fig. 17 Upper subplot shows movement from an extensometer where the line colour indicates the temperature in 2 m at the bunker borehole. The lower subplot shows borehole temperatures at 0, 1, and 2 m depth

modelled for the main body of Veslemannen were in November–December, due to the delay in heat transfer. However, the surface typically freezes in late October, and from that time, Veslemannen more or less stopped moving.

Interestingly, the close coupling between precipitation and movement was less clear in the last stages before the 2019 rock mass fall. Some of the rock falls that triggered accelerations in 2018 and 2019 occurred independently of rain events. The acceleration starting on August 23, 2019, was not caused by rainfall, similar to the last acceleration at Preonzo before it failed in 2012 (Loew et al. 2017).

Comparison with other rockslides

The movements in Veslemannen prior to failure were extraordinarily large compared to other monitored large unstable rock slopes in Norway. The yearly displacement was more than 6 m in the upper part, both in 2018 and in 2019, and peak velocities of more than 1 m/day were measured. In comparison, the largest annual movement in the other high-risk slopes are 0.06–0.08 m (Åknes), 0.05 m (Gamanjinni), and 0.025 m (the main part of Mannen). Veslemannen moved 100 times faster than these sites in the last years preceding the failure. However, these other sites have yet not been in any accelerating stages.

In an international perspective, the velocities that were recorded at Veslemannen are not uncommon. For instance, the Mont la Saxe landslide in Italy is moving in a seasonal pattern like Veslemannen, but it has its main acceleration phases in spring rather than in autumn, as it is probably less affected by deep seasonal frost. A part of the La Saxe reached a maximum velocity of 12 m/day during a crisis and before partly failing in 2014 (Bertolo 2017). The year before, the peak slope deformation

reached 0.17 m/day, and similar velocities were frequently measured at Veslemannen the last years. La Saxe is characterized by weak schists compared to the more competent gneissic rocks at Veslemannen, leading to potentially very different kinematics. It is reasonable to believe that the sliding material in La Saxe has more cohesive strength and can thus accommodate large movements before collapsing. As for Veslemannen, the velocities of La Saxe were also measured by a LiSALab GB InSAR system, but they used a shorter rail in the final stage and were therefore able to measure higher velocities before phase wrapping occurred. At the final stage, the maximum velocity measured will depend on the type of monitoring equipment and frequency of recordings. Loew et al. (2017) reported movements of more than 1 m in the final year prior to the failure of the 2012 Preonzo (210,000 m³) rockslide in Switzerland. This rockslide was developed in brittle bedrock like Veslemannen and its velocity fluctuated both seasonally and in response to precipitation events. Prior to its 2017 3 million m³ failure, annual displacements at Piz Cengalo were around 0.04 to 0.06 m in 2012–2015 and the displacements increased significantly in 2016 and 2017 (Walter et al. 2020).

Risk management and failure forecasting using inverse velocity

Failure forecasting by the inverse velocity method was used relatively uncritically during the first evacuation of Veslemannen in October 2014. With the behaviour that subsequently became apparent, characterized by several annual accelerations connected to rainfall, the method seemed of little practical value. Management and hazard levels onwards were set from velocity threshold values in different sectors of the rockslide, and these were annually adjusted. Due to the rapid response to precipitation, sometimes

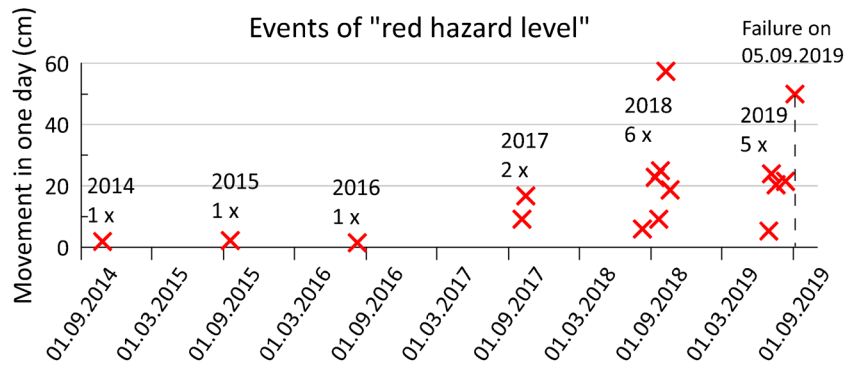


Fig. 18 All reported red hazard levels from 2014 to 2019. The maximum daily displacement measured at radar point 1 during each event is shown on the Y-axis. The movement on the final day is very much underestimated, as phase wrapping in the upper slope affected the radar signal most of this day. Most of the events occurred in autumn, though in 2018 and 2019, the accelerations started earlier

the weather forecast was used when setting the hazard level, to avoid evacuations during night-time. The management and the burden on the evacuated residents became difficult, as a total of 16 evacuations were undertaken. A time series plot of the 16 reported red hazard levels is shown in Fig. 18.

The gentle acceleration that started on August 23, 2019 (Fig. 10) was not triggered by rain. This acceleration caused NVE to change the hazard level from yellow to orange on August 28 and further increase to red hazard level on August 31. The railroad remained open, with a special routine where the police, the train driver, and NVE were on a conference call during each train passage allowing for careful monitoring of the slope during the passages. From the afternoon on September 4, the railroad was closed.

Plotting inverse velocity in the final stage was used more frequently, though still not used as a criterion for setting the hazard levels. Two inverse velocity plots with different time intervals (selected after the event) are shown in Fig. 19. The estimated failure times and correlation coefficient for the two inverse velocity plots are listed in Table 2.

The inverse velocity plot for the first acceleration points to a failure 12–42 h later than when it occurred. For the rain-induced acceleration on September 5, the extrapolation for all three points indicates a failure time around 16:00 the same day, 5 h before it happened. We assume that both indicated times of failure were credible and the discrepancies are a result of changes in basal conditions caused by the rainfall on the day of the failure. This suggests that the failure was most likely imminent regardless of the rainfall on September 5, but that the rainfall forwarded the event a little. As the driving mechanism towards the final failure was reduced when it stopped raining, the failure was slightly delayed. The selected points show a similar pattern, though the noise level is higher for P6 (toe area) as the velocities here were lower than higher in the slope. As we interpret the toe as the controlling part, where breakage of rock bridges was required for the failure to occur, the use of the inverse velocity method should probably focus on this part. Failure forecasting in real time using the inverse velocity model is not always straight-forward, though in retrospect it may be easy to fit a line to the data points pointing to the time of failure.

Important aspects and behaviour of the slopes were learned along the way. Decision-making is required while key elements in the geological understanding are probably missing and may be difficult or impossible to obtain. For Veslemannen, the velocity threshold values used for setting appropriate hazard levels were adjusted at least annually and were typically increased. With experience, our focus shifted from displacements measured in the upper part to the controlling toe area of the instability when evaluating the slope. Despite significant increases in threshold values, the ever-increasing velocities caused many evacuations in 2018 and 2019 (Fig. 18).

With a total of 16 warnings of red hazard levels and evacuations; 15 events could be said to be “false alarms”. NVE was issuing the warnings as “high hazard of rock avalanche” rather than a forecast of the event itself and does therefore not consider the warnings as false. The nature of landslide behaviour may be very different from case to case, which should guide the hazard management. The challenge for deciding hazard level is the uncertainty connected to the time window for the phase leading up to the final collapse, a well-known problem in landslide forecasting. This normally leads to a series of phases with red hazard levels and evacuations before the actual collapse. In cases where the consequences are large, some unnecessary evacuations may be preferred to not issuing red hazard level prior to failure. In this challenging situation, a priority was given to the risk communication towards the evacuated people, the municipality, the police being responsible for the evacuation, and the media. The time and resources used on this aspect promoted a tight interaction and trust between the actors and the evacuated people, and this was the main reason that the early-warning system with hazard warnings and evacuations, after, all were accepted.

If we had the knowledge we have today, the Veslemannen events could have been managed differently, possibly by constructing physical mitigation measures early after its discovery. The early-warning system needs to cope with large uncertainties connected to controlling geological structures and landslide behaviour, which lies in the nature of handling landslide risk. An aim should be to continuously increase the geological understanding while managing this type of risk, so the decision-making is based

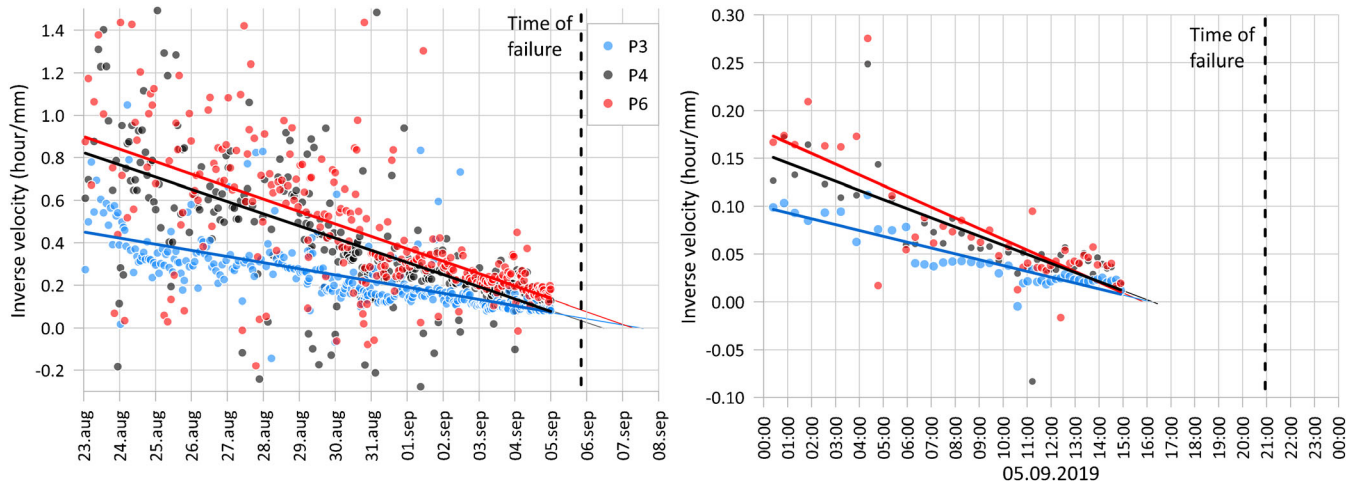


Fig. 19 Inverse velocity plots for selected radar points, where P3 is in the upper part of the slope and P6 is at the toe area. The first plot starts on August 23 and stops when the rain-induced additional acceleration starts (September 5 at midnight). The second plot starts at midnight on September 5 and ends at 15:00 h, where consistent phase wrapping started. Velocities from averages of five GB InSAR images were used to reduce the noise. Linear regression lines are shown and extrapolated to 0 on the Y-axis

on the best available knowledge. We welcome further research use of the different datasets acquired. Some are included in the supplementary material, while other will be supplied on request.

Conclusions

The 5-year monitoring and early warning of the active unstable rock slope Veslemannen have given important new knowledge. These are both on local controlling mechanisms, the understanding of active landslides in general, and for risk management. From this case study, the following major conclusions could be drawn:

- Veslemannen (54,000 m³) failed catastrophically September 5, 2019, after several years with acceleration related to precipitation events. Maximum daily displacement increased from about 5 cm (2014 to 2016) to more than 60 cm (2018 and 2019). The total displacement from 2014 to the failure was up to 19 m in the upper parts and 4–5 m in the toe area.
- The major precursor accelerations occurred exclusively during late summer/fall in relation to precipitation events, while precipitation events earlier in the year or spring snowmelt did not cause such accelerations. We conclude that the influence of possible permafrost and certainly deep seasonal frost strongly controlled the seasonal timing of the acceleration events, as a frozen layer prevented water to reach the sliding zone earlier in the season.
- Numerical modelling of the thermal regime indicates permafrost and/or deep seasonal frost in the landslide. A transition from a possible permafrost to a seasonal frost setting of the landslide body after 2000 was modelled, which may have affected the long-term slope stability.
- The observed changes in the displacement pattern, where larger movements in the upper parts and smaller movements in the toe of the slope evolved towards a more uniform displacement, seem to indicate that the slope is close to collapse. The change may imply that enough structural damage to the confining toe area had occurred allowing for a catastrophic failure to take place.
- The inverse velocity method for failure forecasting should be used with caution, especially in stages where the landslide dynamics is strongly controlled by both external forcing (pore water pressure) and geological/structural conditions. Inverse velocity seems to be more valuable in a late stage when the landslide is moving more uniformly. While this information is useful in back-analysis, forward forecasting is still challenging.
- A high priority should be given to the risk communication, which is necessary for building trust in the early-warning system. The difference between issuing a high (red) hazard level and forecasting a landslide must be communicated clearly. Given the potentially serious consequences of a catastrophic failure, some unnecessary evacuations may be preferred to not issuing a red hazard level prior to a failure.

Table 2 Estimated time of failure at three radar points from the two inverse velocity plots

Plot period	P3	P4	P6
23.08 00:00–05.09 00:00	07.09 14:26 (R: 0.67)	06.09 8:45 (R: 0.69)	07.09 8:32 (R: 0.65)
05.09 00:00–05.09 15:00	05.09 16:04 (R: 0.90)	05.09 16:13 (R: 0.77)	05.09 15:47 (R: 0.79)

Acknowledgements

The authors thank the technical and geological groups at the Section for Rockslide Management at NVE for the effort to provide continuous data for Veslemannen in difficult conditions. We thank the Geohazard and earth observation team at the Norwegian Geological Survey for discussions and support in the data analysis and interpretation, and for providing geological background information. Our equipment suppliers, in particular LiSALab Ellegi (ground based InSAR) and Geopraevent (automatic deformation analysis camera), are thanked for excellent support and help with data analysis. NVE also wish to thank the local authorities for corporation and support in the risk management for Veslemannen: Rauma Municipality, the County Governor in Møre og Romsdal, the police, and the Norwegian Civil Defence. The local inhabitants are thanked for their patience while being severely affected. We acknowledge the canton of Valais and the OFEV (Switzerland) for their support on the activities linked with *Monitoring High Mountain Instabilities* (MIHM). We thank the two reviewers, Simon Löw and Ben Mirus, for their very detailed reviews and critical comments, which considerably improved the overall quality of the original submission.

Funding

The monitoring and analysis were financed by NVE (The Norwegian Water Resources and Energy Directorate), either by internal funding or by research project with the partners at NGU, UiO, and CREALP. The numerical ground temperature modelling was carried out at UiO and funded by UiO and the RCN-funded CRYOWALL project (“Permafrost slopes in Norway”, grant number 243784/CLE).

Data availability

We included the monitoring data and meteorology in the supplementary material. Point clouds, time-lapse images, and other data from the paper are available on request. A further description of the temperature modelling and some movies showing temperature evolution and movie(s) showing large rock falls before the failure is in the supplementary material.

Compliance with ethical standards

Conflict of interest The authors declare that they have no conflict of interest.

Code availability Not applicable

Open Access This article is licensed under a Creative Commons Attribution 4.0 International License, which permits use, sharing, adaptation, distribution and reproduction in any medium or format, as long as you give appropriate credit to the original author(s) and the source, provide a link to the Creative Commons licence, and indicate if changes were made. The images or other

third party material in this article are included in the article's Creative Commons licence, unless indicated otherwise in a credit line to the material. If material is not included in the article's Creative Commons licence and your intended use is not permitted by statutory regulation or exceeds the permitted use, you will need to obtain permission directly from the copyright holder. To view a copy of this licence, visit <http://creativecommons.org/licenses/by/4.0/>.

References

- Abellan A, Kristensen L, Jaboyedoff M et al (2017) Real-time forecasting of slope kinematics in response to precipitation. Application To Veslemannen (SW Norway). In: Proceedings of the progressive rock slope failure. International Society for Rock Mechanics and Rock Engineering, Ascona
- Aleotti P (2004) A warning system for rainfall-induced shallow failures. *Eng Geol* 73:247–265. <https://doi.org/10.1016/j.enggeo.2004.01.007>
- Bertolo D (2017) A decision support system (DSS) for critical landslides and rockfalls and its application to some cases in the Western Italian Alps. *Nat Hazards Earth Syst Sci Discuss*:1–31. <https://doi.org/10.5194/nhess-2017-396>
- Blikra LH, Christiansen HH (2014) A field-based model of permafrost-controlled rockslide deformation in northern Norway. *Geomorphology* 208:34–49. <https://doi.org/10.1016/j.geomorph.2013.11.014>
- Böhme M, Hermanns RL, Gosse J, et al. (2019) Comparison of monitoring data with paleo-slip rates: cosmogenic nuclide dating detects acceleration of a rockslide. *Geology* 47:339–342. <https://doi.org/10.1130/G45684.1>
- Carlà T, Intrieri E, di Traglia F, et al. (2017) Guidelines on the use of inverse velocity method as a tool for setting alarm thresholds and forecasting landslides and structure collapses. *Landslides* 14:517–534. <https://doi.org/10.1007/s10346-016-0731-5>
- Coe JA, Bessette-Kirton EK, Geertsema M (2018) Increasing rock-avalanche size and mobility in Glacier Bay National Park and Preserve, Alaska detected from 1984 to 2016 Landsat imagery. *Landslides* 15:393–407. <https://doi.org/10.1007/s10346-017-0879-7>
- Crosta GB, Agliardi F (2003) Failure forecast for large rock slides by surface displacement measurements. *Can Geotech J* 40:176–191. <https://doi.org/10.1139/t02-085>
- Crosta GB, di Prisco C, Frattini P, et al. (2013) Chasing a complete understanding of the triggering mechanisms of a large rapidly evolving rockslide. *Landslides* 11:747–764. <https://doi.org/10.1007/s10346-013-0433-1>
- Dabrowski M, Krotkiewski M, Schmid DW (2008) MILAMIN: MATLAB-based finite element method solver for large problems. *Geochem Geophys Geosyst* 9. <https://doi.org/10.1029/2007GC001719>
- Dahle H, Saintot A, Blikra LH, Anda E (2010) Geofagleg oppfølging av ustabil fjellparti ved Mannen i Romsdalen. Trondheim. NGU report 2010.022
- Dalsegg E, Rønning JS (2012) Geofysiske målinger på Mannen i Rauma kommune. Møre og Romsdal, Trondheim. NGU report 2012.024
- Fukuzono T (1985) A method to predict the time of slope failure caused by rainfall using the inverse number of velocity of surface displacement. In: Proceedings, 4th International Conference & Field Workshop on Landslides. Tokyo, Tokyo, pp 145–150
- Gruber S, Haerberli W (2007) Permafrost in steep bedrock slopes and its temperature-related destabilization following climate change. *J Geophys Res* 112:F02S18. <https://doi.org/10.1029/2006JF000547>
- Haerberli W (1973) Die Basis-Temperatur der winterlichen Schneedecke als möglicher Indikator für die Verbreitung von Permafrost in den Alpen. *Zeitschrift für Gletscherkunde und Glaziologie* 9:221–227
- Henderson I, Saintot A (2007) Fjellskredundersøkelser i Møre og Romsdal. Trondheim. NGU report 2007.043
- Hilger P, Hermanns RL, Gosse JC et al (2018) Multiple rock-slope failures from Mannen in Romsdal Valley, western Norway, revealed from Quaternary geological mapping and ¹⁰Be exposure dating. *Holocene* 28:1841–1854. <https://doi.org/10.1177/0959683618798165>
- Hilger P, Hermanns RL, Czekirda J, Myhra KS, Gosse JC, Etzelmüller B (2021) Permafrost as a first order control on long-term rock-slope deformation in (Sub-) Arctic Norway. *Quat Sci Rev* 251:106718. <https://doi.org/10.1016/j.quascirev.2020.106718>

- Hughes ALC, Gyllencreutz R, Lohne ØS, et al. (2016) The last Eurasian ice sheets - a chronological database and time-slice reconstruction, DATED-1. *Boreas* 45:1–45. <https://doi.org/10.1111/bor.12142>
- Krautblatter M, Funk D, Günzel FK (2013) Why permafrost rocks become unstable: a rock-ice-mechanical model in time and space. *Earth Surface Processes and Landforms* 38:876–887. <https://doi.org/10.1002/esp.3374>
- Loew S, Gschwind S, Gischig V, et al. (2017) Monitoring and early warning of the 2012 Preonzo catastrophic rock slope failure. *Landslides* 14:141–154. <https://doi.org/10.1007/s10346-016-0701-y>
- Magnin F, Etzelmüller B, Westermann S, et al. (2019) Permafrost distribution in steep rock slopes in Norway: measurements, statistical modelling and implications for geomorphological processes. *Earth Surface Dynamics* 7:1019–1040. <https://doi.org/10.5194/esurf-7-1019-2019>
- Mergili M, Jaboyedoff M, Pullarello J, Pudasaini SP (2020) Back calculation of the 2017 Piz Cengalo–Bondo landslide cascade with r.avaflow: what we can do and what we can learn. *Nat Hazards Earth Syst Sci* 20:505–520. <https://doi.org/10.5194/nhess-20-505-2020>
- Myhra KS, Westermann S, Etzelmüller B (2017) Modelled distribution and temporal evolution of permafrost in steep rock walls along a latitudinal transect in Norway by CryoGrid 2D. *Permafrost Periglacial Process* 28:172–182. <https://doi.org/10.1002/ppp.1884>
- Oppikofer T, Bunkholt H, Ganerød GV, Engvik A (2012) Mannen unstable rock slope (Møre og Romsdal): geological and engineering geological logging of drill core KH-02-11 and grain size distribution and XRD analysis of fine-grained breccia. Trondheim. NGU report 2012.036
- Robertson EC (1988) Thermal properties of rocks.
- Saintot A, Henderson IHC, Derron MH (2011) Inheritance of ductile and brittle structures in the development of large rock slope instabilities: examples from western Norway. *Geol Soc Spec Publ* 351:27–78. <https://doi.org/10.1144/SP351.3>
- Saintot A, Oppikofer T, Derron M-H, Henderson I (2012) Large gravitational rock slope deformation in Romsdalen Valley (Western Norway). *Rev Asoc Geol Argentina* 69:354–371
- Saito M (1969) Forecasting time of slope failure by tertiary creep. In: 7th international conference on soil mechanics and foundation engineering. Mexico, pp. In: 677–683
- Skrede I, Kristensen L, Hole J (2015) Geologisk evaluering av Veslemannen - eit mindre fjellskred i utvikling, Oslo. NVE report 2015.41
- Slagstad T, Balling N, Elvebakk H, et al. (2009) Heat-flow measurements in Late Palaeoproterozoic to Permian geological provinces in south and central Norway and a new heat-flow map of Fennoscandia and the Norwegian-Greenland Sea. *Tectonophysics* 473:341–361. <https://doi.org/10.1016/j.tecto.2009.03.007>
- Voight B (1989) A relation to describe rate-dependent material failure. *Science* 243:200–203. <https://doi.org/10.1126/science.243.4888.200>
- Walter F, Amann F, Kos A, et al. (2020) Direct observations of a three million cubic meter rock-slope collapse with almost immediate initiation of ensuing debris flows. *Geomorphology* 351:106933. <https://doi.org/10.1016/j.geomorph.2019.106933>
- Westermann S, Schuler TV, Gisnås K, Etzelmüller B (2013) Transient thermal modeling of permafrost conditions in Southern Norway. *Cryosphere* 7:719–739. <https://doi.org/10.5194/tc-7-719-2013>

Supplementary Information The online version contains supplementary material available at <https://doi.org/10.1007/s10346-020-01609-x>.

L. Kristensen (✉) · **L. H. Blikra** · **I. Skrede** · **S. Oldani**

The Norwegian Water Resources and Energy Directorate (NVE), Trondheim, Norway
Email: lkr@nve.no

J. Czekirda · **B. Etzelmüller**

The University of Oslo (UIO), Department of Geosciences, Oslo, Norway

I. Penna · **P. Nicolet** · **J. S. Pullarello**

Geological Survey of Norway (NGU), Trondheim, Norway

A. Abellan

University of Leeds, Leeds, England

A. Abellan

Centre for Research on the Alpine Environment (CREALP), Sion, Switzerland